SEISMIC PERFORMANCE OF FRAMES WITH STEEL-CONCRETE COMPOSITE BEAMS: EXPERIMENTAL AND THEORETICAL INVESTIGATION

W.C. Xue[1], J. Li, L. Li and K. Li

[1]*Department of Building Engineering*
Tongji University, Shanghai, China
Email: xuewc@mail.tongji.edu.cn; Fax: +86-21-65986435; Tel: +86-21-65980418

ABSTRACT: This paper aims to study the seismic performance of moment-resisting frames consisting of steel-concrete composite beams subjected to reversed cyclic displacement. The failure patterns, failure mechanism, hysteretic model, deformation-restoring behavior, displacement ductility and energy dissipation capacity of the composite frames are discussed. Hinge is first formed at the composite beam ends. Failure of the two frames under low cyclic displacement reversals is finally governed by crushing and spalling of concrete at top and bottom of columns. Studies also show that the composite frames behave in a ductile manner, and the seismic performance of the composite frames can be significantly improved by the steel-concrete composite beams. In addition, a modified program is employed for full-range analysis of the composite frames.

Keywords: steel-concrete composite beam, frame, seismic performance, failure mechanism, hysteretic model, ductility, energy dissipation, full-range analysis

1. INTRODUCTION

The composite beams show good loading capacities due to composite action between concrete slabs and steel beams through shear connectors. In recent years, many studies focused on the moment resisting frames consisting of composite beams. Previous studies investigated the static behavior (Kennedy & Grace [1], Kocsis [2], Ayyub [3], Li et al [4], Nie & Shen [5], Asta & Dezi [6]) and seismic behavior of steel-concrete composite beams (Nie et al [7] and Xue et al [8]) and composite frames (Thermou et al [9] and Bursi et al [10]). However, few attentions have been paid to investigate the influence of prestressing in composite beams on the seismic performance of frames. This paper aims to investigate the seismic performance of frames with nonprestressed or prestressed composite beams according to low reversed cyclic loading tests and FEM analysis.

2. TEST SETUP

2.1 Design of specimens

Two frames were tested, in which one is fabricated with nonprestreesed steel-concrete composite beams (denoted as syf-1) and the other is fabricated with post-tensioned prestressed steel-concrete composite beams (denoted as syf-2). Details of the two frames are presented in Table 1 and Figure 1.

The two one-story one-bay frames were identical in dimensions, with beam span of 4800mm and column height of 1750mm. All composite beams have the span-to-depth ratio of 16 and depth of 300mm.

Table 1. Details of the two composite frames

Specimens	syf-1	syf-2
Externally prestressed tendons in steel beams	—	$6\phi^s5$
Unbonded tendons in slabs	—	$8\phi^s5$
Steel bars in slabs	Double 7Φ12	Double 7Φ10
Thickness of slabs (mm)	600	600
Spacing of stud connectors (mm)	100	100

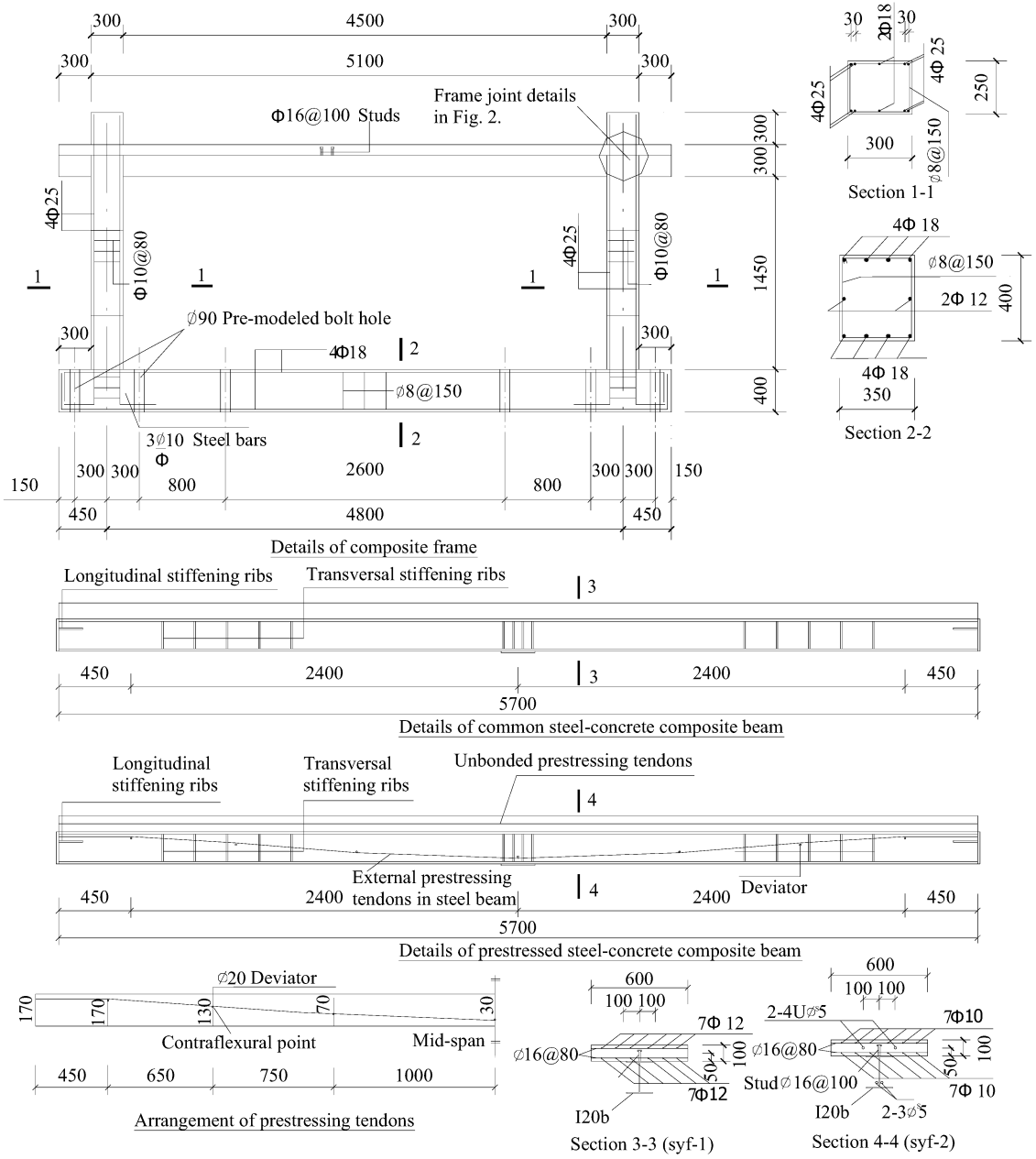

Figure 1. Details of the two composite frames

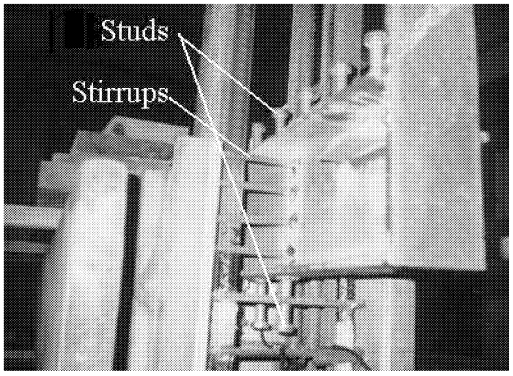

Figure 2. Details of the frame joint

Both frames were casted with C40 concrete. A3 steel was used for steel beams and 16Mn steel with yield stress of 480MPa was used for stud connectors. Steel tendons and five types of steel bars were also used. Mechanical properties of these materials were tested and presented in Table 2 and 3.

Table 2. Mechanical properties of reinforcing bars

Material Properties	A3 steel	Steel bars					Steel tendons
		Φ6	Φ10	Φ12	Φ18	Φ25	Φ^s5
Yield stress (f_y) (N/mm^2)	301.09	361	313	331	359	346	
Ultimate stress (f_u) (N/mm^2)	445.72	498	441	517	527	532	f_{ptk}=1824
Modulus of elasticity E_s (N/mm^2)	1.93 x10^5	2.11 x10^5	1.37 x10^5	1.48 x10^5	1.69 x10^5	1.73 x105	1.89 x10^5
Elongation (%)	27.8	22.3	22.5	24.8	21.6	19.8	13.2

Table 3. Mechanical properties of concrete

Mechanical properties	Cylinder compressive strength f_c (N/mm^2)	Cube compressive strength f_{cu} (N/mm^2)	Modulus of elasticity E_c (N/mm^2)
Concrete (C40)	33.94	50.36	3.36×10^4

2.2 Testing and Measurements

The two frames were tested under reversing lateral displacement and are shown in Figure 3. Axial compression ratios of columns and vertical loads of beams were determined in accordance with the construction practices. Here, the axial compression ratio is defined as

$$\mu_0 = \frac{N}{f_c \cdot A} \tag{1}$$

where μ_0 is the axial compression ratio, N is the axial load, f_c is the cylinder compressive strength of concrete and A is the area of column cross-section.

The lateral displacements, simulating seismic loads, were cyclically applied by using hydraulic actuators. All frames were loaded to failure. Figure 4 shows the loading history of the reversed cyclic load tests. The first cycle was load-controlled, in which frames were loaded until cracks were formed at top of columns. The load corresponding to the first cracking of frames was defined as P_{cr}. The subsequent cycles were displacement-controlled, in which beams were displaced to Δ_y for each cycle. Here, Δ_y is the yield displacement at top of columns, which corresponds to the yielding of the

composite frames. All frames were loaded three cycles in every levels of displacement. Thus, these displacements were arranged in successive sets of cycles, namely as $+1\Delta_y$、$-1\Delta_y$、$+2\Delta_y$、$-2\Delta_y$、$+3\Delta_y$、$-3\Delta_y$……, being multiples of Δ_y.

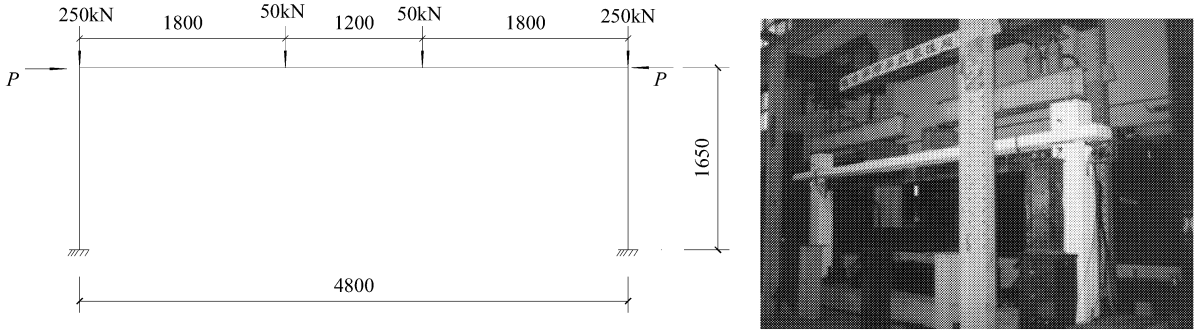

Figure 3. Loading of frames

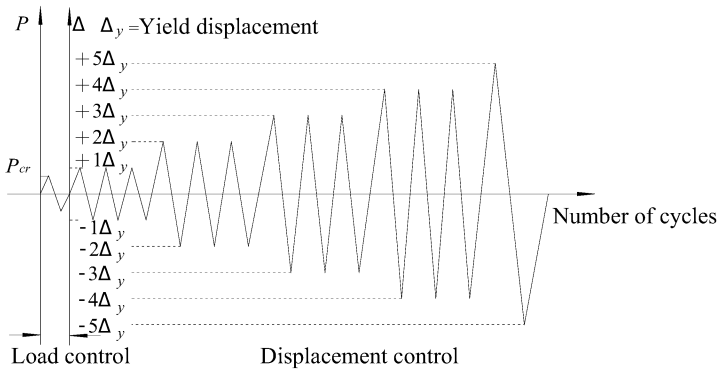

Figure 4. Loading history (Δ_y=H/400; H is the height of column)

The followings were measured and recorded: (1) the lateral load versus lateral drift curves (P-Δ curves); (2) strains of steel beams, longitudinal steel bars in beams and columns, externally prestressed tendons, unbonded prestressed tendons and stirrups in joint cores; (3) slippage between steel beams and concrete slabs; (4) strains of concrete at beam and column ends.

3. TEST OBSERVATIONS

First signs of failure in the two frames were the cracks at top of left columns (as shown in Figure 1) when the lateral load reached 89kN. Compared to specimen syf-1, fewer cracks could be observed in concrete slabs of specimen syf-2 due to the effect of prestressing. Local concrete crushed at bottom of columns in syf-1 when the lateral drift reached $8\Delta_y$, while concrete crushed at bottom columns of syf-2 when the lateral drift reached $10\Delta_y$. For specimen syf-1, concrete spalled at joint cores and column roots. Further slippage was observed between steel beams and concrete slabs. However, concrete spalled at joint cores in syf-2 when the lateral drift reached $14\Delta_y$. Conclusions could be drawn that the specimen syf-1 failed earlier than syf-2. Slippage of the steel beams from the concrete column in syf-1 was greater than that of in syf-2.

It can be observed that failure patterns of the two frames are characterized by first hinging in composite beam ends and then the column ends. Figure 5 and Figure 6 show failures of the two frames.

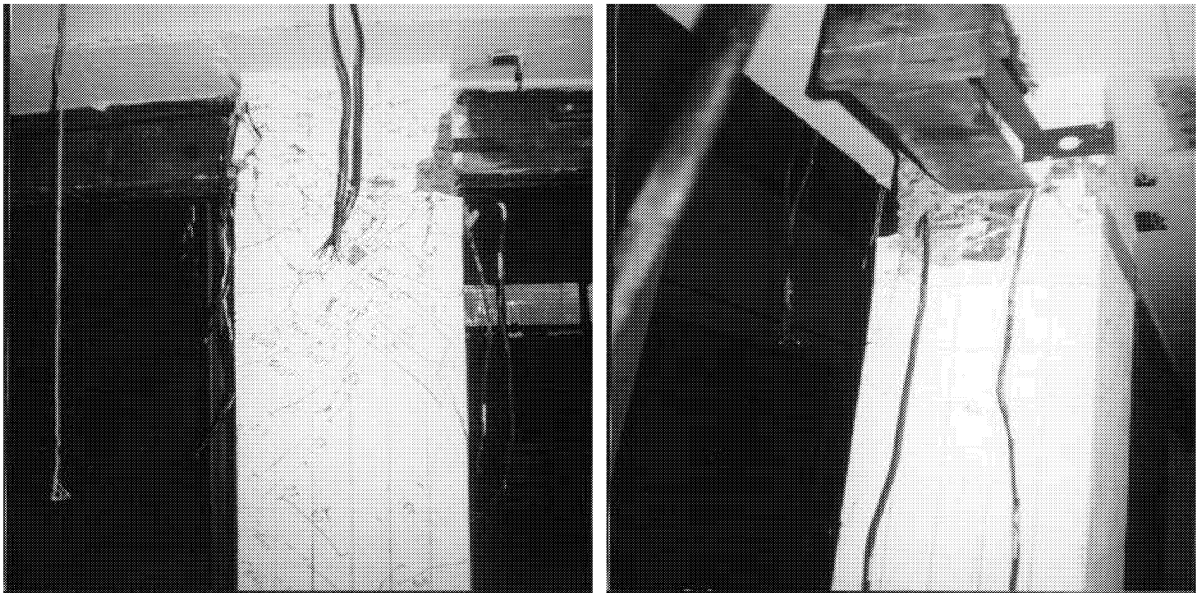

Figure 5. Failure of frame joints

Figure 6. Failure of frame columns

4. TEST RESULTS AND ANALYSIS

4.1 Hysteresis curves

Lateral load versus lateral drift (P-Δ) curves of the two frames are shown in Figure 7. Here, P and Δ are lateral load and lateral displacement at top of frames during testing. It could be observed that hysteresis curves of the two frames are quite similar. Relationship between lateral loads and lateral drift are basically linear before first cracking in frames. Very little residual deformation could be observed, displaying that the two frames are still in elastic ranges at this stage.

Hysteresis loops become curved after cracks occur in frames. Slopes of the two hysteresis curves degrade with increasing lateral drifts. The hysteresis areas become larger gradually. This is called the elasto-plastic stage of the two frames with stiffness degrading in both frames. One of the attributed factors to stiffness degradation is the cumulated damage during the cyclic displacement

reversals. The increasing speed of the lateral loads reduces with increasing lateral drifts. Shapes of hysteresis curves for the two frames in a single loading cycle are quite similar to parallelograms due to hysteretic characteristics of steel beams under cyclic loads.

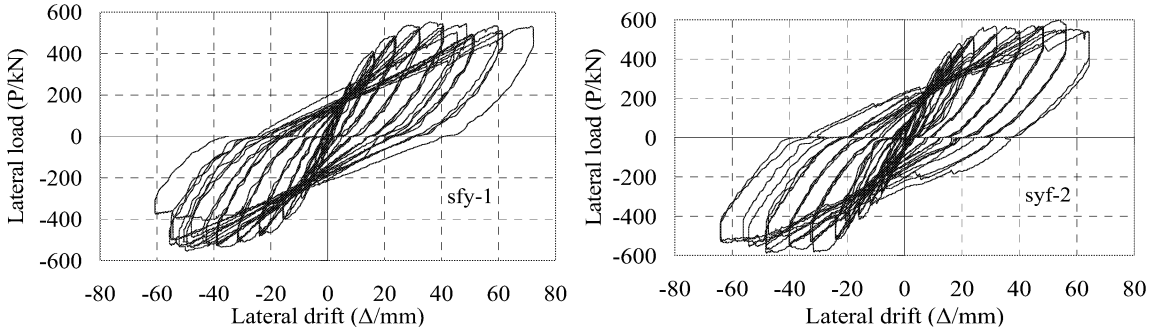

Figure 7. P-Δ curves of the two composite frames

4.2 Skeleton curves

As shown in Figure 8, the two specimens undergo the three point response when subjected to cyclic displacement reversals, namely they are the cracking point, the yield point and the maximum load point. Skeleton curves of both frames are basically linear before the first cracking in frames. After cracking, the load versus lateral displacement relationship becomes curved. This process continues until yielding of the frame, in which an obvious inflexion point could be observed in the skeleton curves. Stiffness of the frames degrades until curves reach the maximum load point. However, loads degrade gradually after the maximum load point.

Skeleton curves of the two frames are quite similar. The applied prestressing and the failure of composite beams have little effect on global seismic behavior of the frame, which can be attributed to the failure patterns of the two frames.

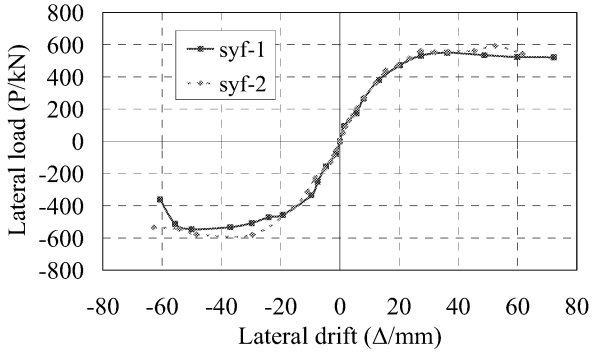

Figure 8. Skeleton curves of frames with composite beams

4.3 Hysteretic model

A four-linear hysteretic model with descending parts and pinching pivot points for hysteresis analysis of the composite frames is obtained on the basis of hysteresis curves, skeleton curves and characteristic loads of the two frames. Figure 9 shows the four-linear hysteretic model for the composite frames, which is characterized by the following hysteretic rules:

(1) The loading stiffness is set equal to the initial stiffness before yielding. Stiffness degradation and residual deformation are not taken into account during unloading.

(2) From the cracking point and the yield point, loading stiffness is assumed to be equal to the post-cracking stiffness and unloading points to the cracking point in the opposite direction.

Stiffness degradation and residual deformation are considered at this loading process.

(3) Between the yield point and the ultimate point, loading stiffness is set to be equal to the post-yield stiffness and assumed to be negative after the ultimate point. The unloading stiffness is taken as K by the reduction factor β. Here, K is the stiffness from the yield point to its corresponding cracking point at opposite direction of loading. The reduction factor is defined as:

$$\beta = (\frac{\Delta_y}{\Delta_m})^{\nu} \tag{2}$$

Where Δ_y is the yield displacement, Δ_m is the previous maximum displacement and ν is the factor obtained from the test results. Then the post yield stiffness K_{py} is defined as:

$$K_{py} = \beta \cdot K \tag{3}$$

(4) The reloading paths in the opposite direction of loading after post-yield unloading directly takes along a line which connects the point at which unloading was completed with the cracking point in the opposite direction of loading provided that the maximum previous displacement in the opposite direction of loading do not exceed the cracking displacement (Δ_{cr}). It can be observed that all load-displacement paths tend to cross at approximately the same point in two loading directions (the points corresponding to the loads P_1 and $-P_1$, as shown in Figure 9). We define these two points as the pinching pivot points. The reloading path takes along a line which connects the point at which unloading was completed with the pinching pivot point in the opposite direction of loading provided that the maximum previous displacement in the opposite direction of loading is between the cracking displacement (Δ_{cr}) and the displacement (Δ_1) corresponding to the pinching pivot point. Provided that the maximum previous displacement in the opposite direction of loading is greater than the displacement corresponding to the pinching pivot point, the reloading paths in the opposite direction of loading takes along a line which connects the following three points: the point at which unloading was completed, the pinching pivot in the opposite direction of loading and the point on the skeleton curve in the opposite direction of loading.

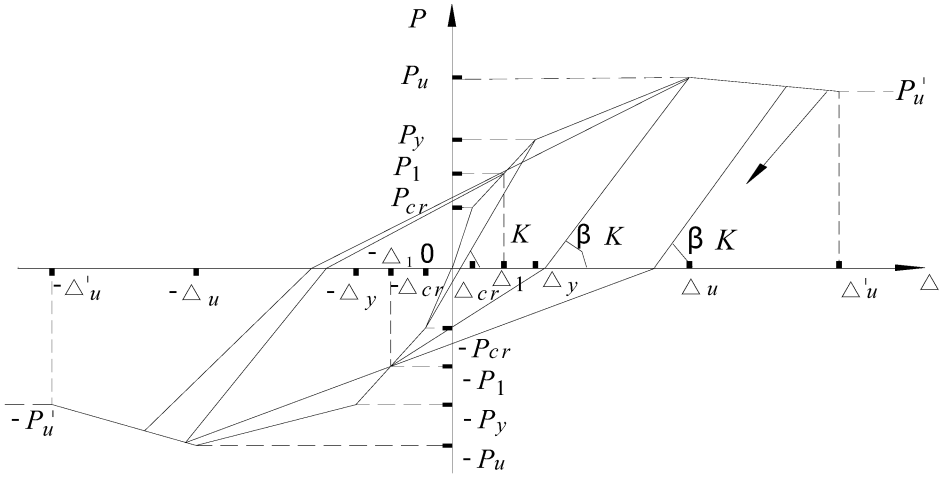

Figure 9. Hysteretic model for composite frames

4.4 Failure mechanisms

Failure of the two frames under cyclic displacement reversals is finally governed by crushing and spalling of concrete at top and bottom of columns. In comparison with the top of columns, the

column roots suffered more serious failure.

Figure 10 shows the sequences of plastic hinge formation in the two composite frames during the testing. Comparisons between the test results and the analytical results calculated by the PK software [11] are presented in Table 4. It can be observed that the tested sequences are in accordance with the results calculated by PK.

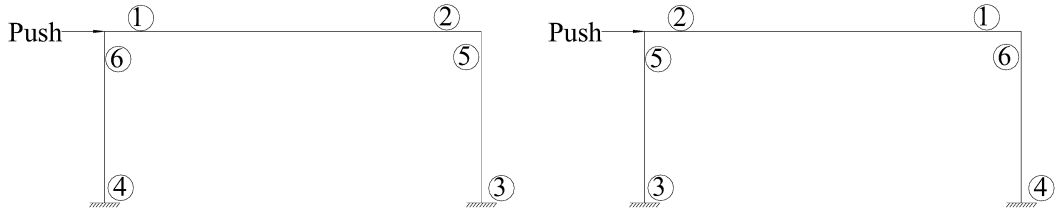

Frame with common composite beams

Frame with externally prestressed composite beams

Figure 10. Sequences of plastic hinge formation in the two frames

Table 4. Lateral loads corresponding to hinge formation

Locations of plastic hinges	Syf-1		Syf-2	
	Experimental values (kN)	Analytical values by PK (kN)	Experimental values(kN)	Analytical values by PK (kN)
Hinging at the beam ends	212	226	194	186
Hinging at the column ends	475	317	501	305
Failure loads	542	417	577	409

The sequences of plastic hinge formation in the two frames are quite similar. Both frames first develop hinge at beam ends and then at root and top of columns. This sequence of hinge formation is in accordance with the strong-column weak-beam criterion, which requires that the flexural strength of columns must be larger than that of the beams. Both frames fail by crushing of concrete at column roots and have been designed to achieve the strong-column weak-beam requirements. This kind of failure mechanism provides the frames with better ductility and larger energy dissipation capacity.

4.5 Deformation restoring capacity

In this paper, residual deformation ratio, which is defined as Δ_r/Δ_u, is used as a key index for evaluating deformation restoring capacity of beam specimens. Here, Δ_r is the residual displacement after unloading and Δ_u is equal to the maximum displacement for skeleton curves without descending part or equal to the displacement corresponding to 85% of the maximum loads in descending part of the skeleton curves. Residual deformation and residual deformation ratios of the two composite frames are presented in Table 5.

Table 5. Residual deformation of the two composite frames

Specimens	Syf-1	Syf-2
Residual deformation Δ_r (mm)	46.55	35.90
Maximum deformation Δ_e (mm)	72.30	63.94
Residual deformation ratio Δ_e/Δ_r	0.64	0.56

As shown in the table, residual deformations and residual deformation ratios of specimen sfy-2 are higher than that of sfy-1, which indicates that frames with externally prestressed composite beams

have larger deformation restoring capacities than that with common composite beams.

4.6 Ductility

Ductility coefficient μ is defined as

$$\mu = \frac{\Delta_u}{\Delta_y} \qquad (4)$$

where Δ_u is the maximum lateral drift, Δ_y is the displacement corresponding to yielding of frames. The displacements and ductility coefficients of the two frames during testing are listed in Table 6.

As shown in Table 6, ductility coefficients of the two frames are quite close to each other. Failure of the two frames mainly occurs at column ends and beam-column joints. Therefore, the composite beams are not decisive factors to failure of the two frames and the prestressing applied in composite beams has little effect on seismic performance of the frames.

Table 6. Ductility coefficients of the two composite frames

Specimens		Syf-1		Syf-2	
Loading direction (show in Figure 3)		←	→	←	→
Cracking displacement	Δ_{cr} (1/100mm)	208	200	80	88
	Δ_{cr}/H	1/793	1/825	1/2062.5	1/1875
Yield displacement	Δ_y (1/100mm)	2386	2380	2410	2408
	Δ_y/H	1/69	1/69	1/68	1/69
Ultimate displacement	Δ_u (1/100mm)	7220	7230	6418	6394
	Δ_u/H	1/23	1/23	1/26	1/26
Ductility coefficient (μ)	Δ_u/Δ_y	3.04	3.04	2.66	2.64

4.7 Energy dissipations

The energy dissipated during a single load cycle is calculated using the Trapezoid Rule to determine the area within lateral load (P) versus lateral drift (Δ) curve. The amount of energy dissipated in the two composite frames is depicted in Figure 11. The following conclusions could be drawn from this figure:

(1) At the early period of loading, the loading paths are nearly linear and little amount of energy has been dissipated in the two frames.

(2) The energy dissipation capacity of the two frames increases with increasing displacements. However, the dissipated energy keeps on decreasing in the three load cycles with identical lateral displacements due to cumulated damage during testing.

(3) The energy dissipation curves of the two frames are very close to each other at initial loading stages.

(4) When the lateral drifts are equal to or higher than $6\Delta_y$, more energy has been dissipated in syf-2 in comparison with that in syf-1.

(5) The amount of energy dissipated in sfy-1 remains as a constant during the loading cycles

with lateral drifts of $12\Delta_y$ and $14\Delta_y$. However, no similar phenomenon occurs in syf-2. The reason is that larger slippage is observed between steel beam and concrete slab in syf-1, which affects the energy dissipation capacity of frames with common composite beams.

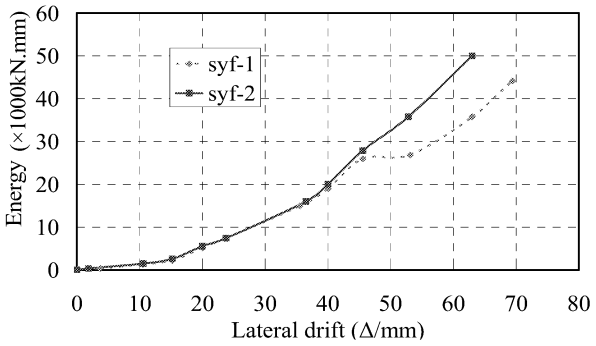

Figure 11. Energy dissipation

4.8 Hysteresis analysis

A modified program based on the FEM theory (Xue & Zhang [12]), simulating the hysteretic behavior of the composite frames, is proposed in the paper. Note that both the nonprestressed and prestressed composite beam elements are incorporated in this program.

The material nonlinearity, geometric nonlinearity and prestressing are main factors that affecting the inelastic response of composite frames with externally prestressed composite beams. The above factors are considered in the proposed program, which is proven to be a better way for full-range analysis of the prestressed composite frames. As shown in Figure 12, each frame is discretized into 20 elements, 5 for a column and 10 for a composite beam. The layered-section approach is employed for element analyses. As shown in Figure 13, the composite beam section is discreted into twenty-three slices: five for concrete, fourteen for steel beams, one for prestressed tendons in steel beams, one for unbonded prestressing tendons in concrete slabs and two for top and bottom longitudinal steel bars in concrete slabs.

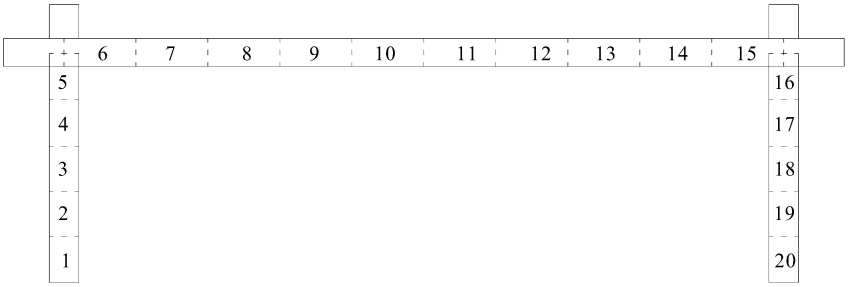

Figure 12. Element discretization for frames

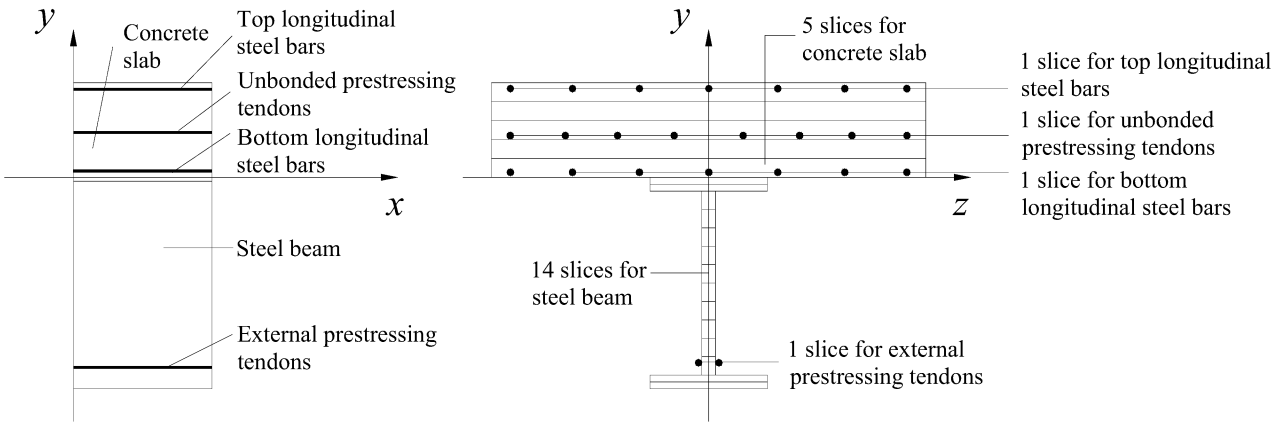

Figure 13. Discretization for composite beam sections

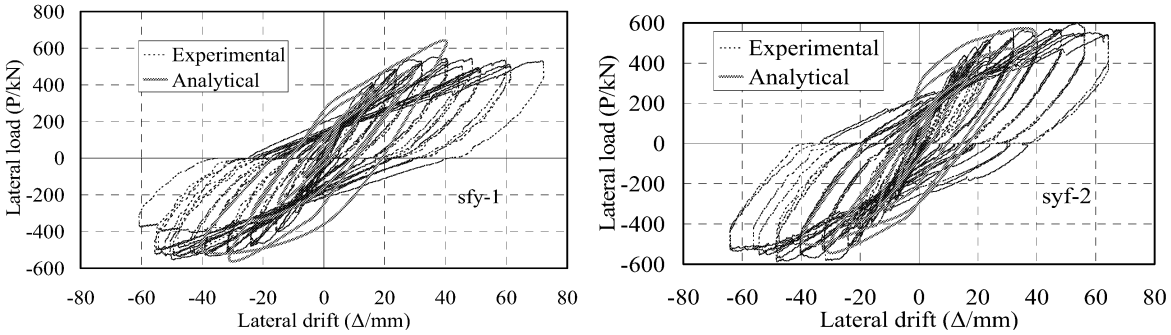

Figure 14. Comparisons of experimental and analytical P-Δ curves for the two frames

Comparison of lateral loads versus lateral drifts curves between experimental and analytical results are shown in Figure 14. By comparing experimental and analytical results of hysteresis curves for the two frames, the following conclusions can be drawn with:

(1) At the early period of the loading, the experimental and the analytical curves are in good agreement.

(2) At the last period of loading, the experimental and the analytical curves are not in good agreement with each other. Deviations of the two curves become larger with increasing displacements. However, their experimental and analytical ultimate loads are similar.

5. CONCLUSIONS

From the studies described in this paper, we can draw the following conclusions:

(1) During testing, plastic hinges first form at beam ends and finally at top and bottom of columns. Failure patterns of the two frames are dominated by crushing and spalling of concrete at top and bottom of columns. More serious failure occurs at bottom of columns. The beam sideway mechanism indicates that the seismic performance of the frames has been significantly improved by the composite beams.

(2) Hysteresis curves for the two frames are relatively full during cyclic loading. Shape of hysteresis loops for the two frames is quite similar, indicating that prestressing applied in composite beams has little influence on seismic behavior of frames.

(3) Displacement ductility coefficients of the two frames are quite close to each other. Tests also show that frames with prestressed composite beams have better deformation restoring capacities.

(4) The amount of energy dissipated in the two frames during the early period of the testing is nearly the same. However, more energy has been dissipated in the frame with externally prestressed composite beams in comparison to that with common composite beams. This can be due to the slippage between the steel beams and the concrete slabs in the frame with common composite beams.

(5) A modified program is proposed and employed for hysteresis analysis of the two composite beams.

(6) Based on investigation of failure patterns, hysteresis curves, ductility and energy dissipation capacity of the two frames, conclusions could be drawn that seismic performance of the two frames could be significantly improved by the composite beams.

ACKNOWLEDGEMENTS

Support for this research by the Shanghai Development Foundation of Science and Technology under Grant No. 992012044 and the "Shu Guang" project supported by Shanghai Municipal Education Commission and Shanghai Education Development Foundation.

REFERENCES

[1] Kennedy, J.B. and Grace, N.F., "Prestressed Continuous Composite Bridges under Dynamic Load", J. Struct. Div., ASCE, 1990, 116(6), pp.1660-1678.
[2] Kocsis, P., "Guidelines for Flexural Design of Prestressed Composite Beams", J. Struct. Div., ASCE, 1990, 117(11), pp.3548-3549.
[3] Ayyub, B.M., Sohn, Y.G. and Saadatmanesh, H., "Prestressed Composite Girders. II : analytical study for negative moment", J. Struct. Div., ASCE, 1992, 118(10), pp.2763-2783.
[4] Li, W.L., Albrecht, P. and Saadatmanesh, H., "Strengthening of Composite Steel-Concrete Bridges", J. Struct. Div., ASCE, 1995, 121(12), pp.1842-1849.
[5] Nie, J.G. and Shen, J.M., "Experimental and Analysis of Actual Shear Capacity of Shear Connectors in Composite Steel-Concrete Beams", Journal of Building Structure, 1996, 117(2), pp.3-9. (in Chinese)
[6] Asta, A.D and Dezi L., "Nonlinear Behavior of Externally Prestressed Composite Beams: analytical model", J. Struct. Div., ASCE, 1998, 124(5), pp.588-597.
[7] Nie, J.G., Yu, Z.L. and Ye, Q.H., "Seismic behavior of composite steel-concrete beams", Journal of Tsinghua University, 1998, 8(10), pp.35~37. (in Chinese)
[8] Xue, W.C., Li, K. and Li, J., "Experimental Studies of Steel-Concrete Composite Beams under Low Reversed Cyclic Loading", Journal of Earthquake Engineering and Engineering Vibration, 2002, 22(6), pp.65-70. (in Chinese)
[9] Thermou, G.E., Elnashai, A.S., Plumier, A. and Doneux, C., "Seismic design and performance of composite frames", Elsevier Ltd, Journal of Construction Steel Research, 2004, 60(1), pp.31-57.
[10] Bursi, O.S., Sun F.F. and Postal, S., "Nonlinear analysis of steel-concrete composite frames with full and partial shear connection subjected to seismic loads", Elsevier Ltd, Journal of Construction Steel Research, 2005, 61(1), pp.67-92.
[11] www.pkpm.com.cn
[12] Xue, W.C. and Zhang, Z.T,. "Method and Application in Nonlinear Full-Range Analysis of Reinforced Concrete", Journal of Computational Mechanics, 1999, 16(3), pp.334-342. (in Chinese)